Inorganic Chemistry

Article

pubs.acs.org/IC

Vacancy Ordering as a Driving Factor for Structural Changes in Ternary Germanides: The New $R_2Zn_{1-x}Ge_6$ Series of Polar Intermetallics (R = Rare-Earth Metal)

Pavlo Solokha,*[,†] Serena De Negri,[†] Davide M. Proserpio,[‡,§] Vladislav A. Blatov,[§] and Adriana Saccone[†]

[†]Dipartimento di Chimica e Chimica Industriale, Università di Genova, Via Dodecaneso 31, 16146 Genova, Italy

[‡]Dipartimento di Chimica, Università degli Studi di Milano, Via Golgi 19, 20133 Milano, Italy

[§]Samara Center for Theoretical Materials Science (SCTMS), Samara State University, Ac. Pavlov Street 1 Samara 443011, Russia

Supporting Information

ABSTRACT: Synthesis and structural characterization of the new compounds $R_2Zn_{1-x}Ge_6$ (R = La–Nd, Sm, Gd–Ho) is reported. A structural change was revealed along this series by careful analysis of single-crystal X-ray diffraction data. For light rare earths up to Tb the orthorhombic *oS*72-$Ce_2(Ga_{0.1}Ge_{0.9})_7$ model was established; instead, the Dy compound represents a new structure type ($P2_1/m$, *mP*34, $Z = 4$, $a = 7.9613(3)$ Å, $b = 8.2480(4)$ Å, $c = 10.5309(5)$ Å, $\beta = 100.861(1)°$) being a superstructure of the *mS*36-La_2AlGe_6 prototype. The established structural models support the increase of Zn deficiency along the series, suggested by microprobe analysis, and its key role in governing structural changes. The vacancy ordering criterion was applied as a successful approach to find a general scheme including the structures of the ~R_2MGe_6 compounds known up to now (R = rare-earth metal, M = transition metal, Mg, Al, Ga) and highlighting the subtle structural differences within this family. According to this scheme, these structures are obtained from a common aristotype (*oS*20-$SmNiGe_3$) via symmetry reduction based on group–subgroup relations accompanied by ordering of vacancies. This approach was optimized with the help of the ToposPro software and extended to the $R_2Zn_3Ge_6$ series, enriched with new members (R = Sm, Gd–Ho) during this work. Electronic structure calculations on La_2ZnGe_6 confirm the presence of infinite covalent germanium zigzag chains and three-bonded corrugated layers connected via Zn atoms to form a polyanionic network stabilized by La atoms.

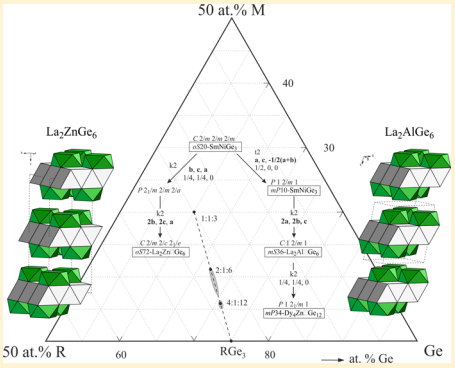

1. INTRODUCTION

Rare-earth-based binary and ternary germanides form a group of polar intermetallics extensively studied with respect to crystal structure, chemical bonding, and physical properties.[1−6] These compounds show a great crystallographic variety, including defective structures,[1,4] superstructures,[3,4] and modulated structures.[5,6] From the point of view of chemical bonding various characteristic Ge-based covalent fragments exist in these compounds, including dumbbells,[7,8] 2D motifs,[9,10] and 3D more complex fragments,[9,11] whose occurrence depends on the Ge concentration. Interesting physical properties, such as giant magnetocaloric effect,[12] superconductivity,[13] anomalous thermal expansion,[6] and others, were also discovered in rare-earth germanides.

Investigations on series of these compounds along the whole lanthanide (R) family[1,14] proved that their existence and structure are influenced by the nature of R, and for this reason they are good candidates for studies of structure/bonding/properties relations. The role of the third component (M) is also of great interest for ternary R–M–Ge compounds.

During our recent investigation of the La–Mg–Ge phase relations the La_2MgGe_6 compound was found, and its structure (*oS*72-$Ce_2(Ga_{0.1}Ge_{0.9})_7$) was established.[4] This compound, which does not form for rare-earth metals other than lanthanum, is a member of the numerous family of R_2MGe_6 phases (R = rare-earth metal; M = transition or main group metal) whose occurrence and crystal structures are summarized in Table 1. The metals M involved in the formation of these compounds range from the 2nd to the 13th group of the periodic table, including many transition metals.

All ~R_2MGe_6 compounds fall into orthorhombic or monoclinic crystal families and are reported to belong to one of the following isostructural series: (a) *oS*18-Ce_2CuGe_6, space group *Amm*2 (No. 38); (b) *oS*72-$Ce_2(Ga_{0.1}Ge_{0.9})_7$, space group *Cmce* (No. 64); (c) *mS*36-La_2AlGe_6, space group *C*2/*m* (No. 12). The metrics of the two orthorhombic models are related: the unit cell of the latter is four times bigger than that of the former. Nevertheless, the correctness of the *oS*18 model is suspicious for two reasons.

(1) This model was always deduced from X-ray powder diffraction patterns, which are not sensitive to small structural differences. In fact, the crystal structures of $(La/Dy/Yb)_2PdGe_6$ and $(La/Dy)_2PtGe_6$, previously

Received: December 21, 2014
Published: February 10, 2015

DOI: 10.1021/ic5030313
Inorg. Chem. 2015, 54, 2411−2424

Table 1. Structure Types of R−M−Ge Compounds of ∼2:1:6 Stoichiometry (R = rare-earth metal; M = metal)[a]

Group	M	R= Y	La	Ce	Pr	Nd	Sm	Eu	Gd	Tb	Dy	Ho	Er	Tm	Yb	Lu	Ref.
2	Mg	–	●	–	–	–	–		–	–	–	–	–		–		4
9	Co	⊠		–	–	–	–	–	⊠	⊠	⊠	⊠	⊠	⊠		⊠	16,17
10	Ni	⊠		⊠	⊠	⊠	⊠	–	⊠	⊠	⊠	⊠	⊠	⊠	⊠	⊠	16, 17
	Pd	⊠ ●	⊠ ●	⊠	⊠	⊠	⊠	⊠	⊠	⊠	⊠ ●	⊠	⊠	⊠	⊠ ●	⊠	16, 17 18, 19
	Pt	⊠	⊠ ●	⊠	⊠	⊠	⊠	⊠	⊠	⊠	⊠ ●	⊠	⊠	⊠	⊠	⊠	16, 17 18
11	Cu	⊠	⊠	⊠	⊠	⊠	⊠	–	⊠	⊠	⊠	⊠	⊠	⊠	⊠		16, 17
	Ag		⊠	⊠	⊠	⊠	⊠	–	⊠			–				–	16, 17
	Au		⊠	⊠	⊠	⊠	⊠	–	⊠	⊠	⊠	–					16, 17
12	Zn		●	●	●	●	●		●	●	○	○	–	–			this work
13	Al	–	◈	◈	◈	◈	◈	–	◈	◈	◈	–	–	–	–	–	16, 17
	Ga	● ◈		●			●	–									16, 20

[a]A blank cell means that an alloy of this composition was not investigated.

reported as *oS*18-Ce_2CuGe_6, were subsequently reinterpreted as *oS*72-$Ce_2(Ga_{0.1}Ge_{0.9})_7$ after single-crystal X-ray diffraction analysis.[18,19]

(2) This model does not agree with the symmetry principle.[15] According to that, atoms of the same kind have the tendency to occupy the minimal number of equivalent positions in a crystal, a condition not satisfied by Ge atoms in the *oS*18 model.

The two models *oS*72 and *mS*36 are also intimately related. In fact, they can be described as belonging to a homological series constructed by linear intergrowth of inhomogeneous segments of the defective $BaAl_4$, AlB_2, and α-Po structure types.[20,21] An alternative description was given by Grin,[22] based on only two types of segments, AlB_2 and defective $CeRe_4Si_2$.

The compositions of many of the above-mentioned R−M−Ge phases are not exactly coincident with the 2:1:6 stoichiometry, being more Ge or M rich. It is the case of two prototypes: in $Ce_2(Ga_{0.1}Ge_{0.9})_7$ a statistical mixture of Ga and Ge in different crystallographic sites leads to a more Ge-rich composition; instead, in La_2AlGe_6 ($La_2Al_{1.6}Ge_{5.4}$) a partial substitution of Ge by Al atoms is reflected in a more Ge-poor composition. In these cases the total number of atoms per unit cell is coincident with the stoichiometric model, but a more correct general formula should be $R_2M_{1-x}Ge_{6+x}$, where x could be positive or negative. For R = Y, M = Ga both possibilities are realized;[20] in fact, two compounds have been reported with these elements, a Ge-rich phase ($Y_2Ga_{0.34}Ge_{6.66}$, *oS*72, x = 0.66) and a Ge-poor one ($Y_2Ga_3Ge_4$, *mS*36, x = −2).

On the basis of these data and considering that no transition elements of group 12 had been taken into account up to now, we decided to explore the existence and crystal structure of an analogous series of R_2MGe_6 compounds where M = Zn. Here, we present the synthesis and structural characterization of the new $R_2Zn_{1-x}Ge_6$ series (R = La−Nd, Sm, Gd−Ho), enriching the 2:1:6 family with a new structure type (found for R = Dy). The role of Zn deficiency in governing structural changes will be particularly discussed. A general group−subgroup relation scheme based on vacancy ordering is also proposed to rationalize the crystal structures inside this family and extended to $R_2Zn_3Ge_6$ compounds. Moreover, results of electronic structure calculations on La_2ZnGe_6 will be presented in order to complete the characterization of these polar intermetallics from the chemical bonding point of view.

2. EXPERIMENTAL SECTION

2.1. Synthesis, Microstructure, and Phase Analysis. Samples of about 0.8 g with $R_{22.2}Zn_{11.1}Ge_{66.7}$ (R = La−Nd, Sm, Gd−Tm) nominal compositions were prepared by direct synthesis from the pure

Table 2. Crystallographic Data for $R_2Zn_{1-x}Ge_6$ (R = La, Ce, Nd, Gd, Tb, Dy) Single Crystals, and Experimental Details of the Structural Determination

empirical formula	$La_2Zn_{1-x}Ge_6$	$Ce_2Zn_{1-x}Ge_6$	$Nd_2Zn_{1-x}Ge_6$	$Gd_2Zn_{1-x}Ge_6$	$Tb_2Zn_{1-x}Ge_6$	$Dy_2Zn_{1-x}Ge_6$
code	*crystal I*	*crystal II*	*crystal III*	*crystal IV*	*crystal V*	*crystal VI*
x (EDXS)	0.011	0.051	0.15	0.33	0.39	0.43
x (structural model)	0.063(6)	0.089(9)	0.156(5)	0.364(6)	0.437(6)	0.50
structure type	$Ce_2(Ga_{0.1}Ge_{0.9})_7$	$Ce_2(Ga_{0.1}Ge_{0.9})_7$	$Ce_2(Ga_{0.1}Ge_{0.9})_7$	$Ce_2(Ga_{0.1}Ge_{0.9})_7$	$Ce_2(Ga_{0.1}Ge_{0.9})_7$	$Dy_2Zn_{1-x}Ge_6$
cryst syst	orthorhombic	orthorhombic	orthorhombic	orthorhombic	orthorhombic	monoclinic
space group	*Cmce* (No. 64)	*Cmce* (No. 64)	*Cmce* (No. 64)	*Cmce* (No. 64)	*Cmce* (No. 64)	$P2_1/m$ (No. 11)
M_w [g/mol]	774.64	775.18	779.18	791.63	790.32	793.22
Pearson symbol, Z	*oS*72−0.50, 8	*oS*72−0.71, 8	*oS*72−1.25, 8	*oS*72−2.91, 8	*oS*72−3.50, 8	*mP*36−2.00, 4
a [Å]	8.7294(9)	8.6498(12)	8.5437(10)	8.3559(10)	8.3041(5)	7.9613(3)
b [Å]	8.2841(8)	8.2578(11)	8.1765(9)	8.0377(10)	8.0053(5)	8.2480(4)
c [Å]	21.483(2)	21.340(3)	21.175(2)	20.876(3)	20.7898(13)	10.5309(5)
β [deg]						100.861(1)
V [Å^3]	1553.6(3)	1524.3(4)	1479.3(3)	1402.1(3)	1382.04(15)	679.12(5)
calcd density [g/cm^3]	6.659	6.756	6.997	7.500	7.870	7.758
abs coeff (μ), mm^{-1}	36.53	37.686	40.358	45.993	49.168	49.481
unique refIns	1021	1307	982	930	1122	2195
refIns $I > 2\sigma(I)$	788 (R_{sigma} = 0.0272)	1133 (R_{sigma} = 0.0235)	904 (R_{sigma} = 0.0135)	509 (R_{sigma} = 0.0313)	813 (R_{sigma} = 0.0125)	1795 (R_{sigma} = 0.0196)
data/parameters	1021/51	1307/50	982/51	930/51	1122/51	2195/100
GOF on F^2 (S)	1.13	1.15	1.29	1.00	1.16	0.98
final R indices [$I > 2\sigma(I)$]	R_1 = 0.0283; wR_2 = 0.0736	R_1 = 0.0537; wR_2 = 0.1585	R_1 = 0.0220; wR_2 = 0.0464	R_1 = 0.0280; wR_2 = 0.0555	R_1 = 0.0242; wR_2 = 0.0496	R_1 = 0.0268; wR_2 = 0.0683
R indices (all data)	R_1 = 0.0371; wR_2 = 0.0790	R_1 = 0.0576; wR_2 = 0.1634	R_1 = 0.0236; wR_2 = 0.0470	R_1 = 0.0639; wR_2 = 0.0678	R_1 = 0.0364; wR_2 = 0.0543	R_1 = 0.0361; wR_2 = 0.0742
$\Delta\rho_{fin}$ (max/min) [e/Å^3]	2.64/−1.91	7.98/−4.91	1.77/−1.19	2.53/−2.53	2.03/−3.24	3.96/−3.08

DOI: 10.1021/ic5030313
Inorg. Chem. 2015, 54, 2411−2424

components (rare-earth metals and zinc were supplied by Newmet Koch, Waltham Abbey, England, and germanium by MaTecK, Jülich, Germany; nominal purities of all metals > 99.9 mass %). The stoichiometric amounts of the pure metals were enclosed in an arc-sealed Ta crucible with the aim to avoid Zn losses due to evaporation. The crucible was then closed in an evacuated quartz vial to prevent oxidation and placed in a resistance furnace where the following thermal cycle was applied: (1) heating (10 °C/min) up to T = 950 °C; (2) cooling down (about 0.5 °C/min) to 350 °C. During the thermal cycle, a continuous rotation, at a speed of 100 rpm, was applied to the vial. Samples were subsequently quenched in cold water. The obtained alloys are very brittle. No tantalum contamination of the samples was observed.

Samples were embedded in a phenolic hot mounting resin with carbon filler. Smooth alloys surfaces suitable for the microscopic examinations were obtained by means of SiC papers and diamond pastes with particle size decreasing from 6 to 1 μm. After each polishing step samples were ultrasonically cleaned for a few minutes in a petroleum ether bath. Microstructure observation and qualitative/quantitative analysis were performed by a scanning electron microscope (SEM) *EVO 40* (Carl Zeiss SMT Ltd., Cambridge, England) provided with a Pentafet Link energy-dispersive X-ray spectroscopy (EDXS) system controlled by the package Inca Energy (Oxford Instruments, Analytical Ltd., Bucks, U.K.). Cobalt standard was used for calibration.

2.2. X-ray Diffraction Measurements. Single crystals of good quality and size were extracted from the mechanically fragmented alloys and selected with the aid of a light optical microscope (Leica DM4000 M, Leica Microsystems Wetzlar GmbH, Welzlar, Germany) operated in the dark field mode. The crystals under analysis, exhibiting metallic luster, were mounted on glass fibers using quick-drying glue. Intensity data have been collected at ambient conditions (295 K) on a four-circle Bruker Kappa APEXII CCD area detector diffractometer equipped with graphite-monochromatized Mo Kα radiation (λ = 0.71073 Å). The instrument was operated in the ω scan mode. Intensity data were collected over the reciprocal space up to ~30° in θ with exposures of 20−30 s per frame. Semiempirical absorption corrections based on equivalents were applied to all data by the *SADABS* software.[23] X-ray diffraction on powder samples was performed by means of a Philips *X'Pert* MPD diffractometer (Cu Kα radiation, step mode of scanning) in order to ensure crystal structures of the studied phases.

Selected crystallographic data and structure refinement parameters for the six studied phases are listed in Table 2. The crystal structure solution, requiring a detailed description, is discussed in section 3.1.

Details on structure refinement can be also found in the Supporting Information in the form of a CIF file. The CIF file has also been deposited with Fachinformationszentrum Karlsruhe, 76344 Eggenstein-Leopoldshafen, Germany: depository numbers CSD-428090 ($La_2Zn_{1-x}Ge_6$-*crystal I*), CSD-428091 ($Ce_2Zn_{1-x}Ge_6$-*crystal II*), CSD-428092 ($Nd_2Zn_{1-x}Ge_6$-*crystal III*), CSD-428093 ($Gd_2Zn_{1-x}Ge_6$-*crystal IV*), CSD-428680 ($Tb_2Zn_{1-x}Ge_6$-*crystal V*), and CSD-428094 ($Dy_2Zn_{1-x}Ge_6$-*crystal VI*). The powder patterns generated from the single-crystal models correspond well to the observed powder diffraction patterns.

2.3. Vacancy Ordering Modeling Basing on Symmetry Principle. The ToposPro[24] software was applied with the goal to deduce structural models related to an aristotype (parent structure) by selected criteria satisfying the symmetry principle.[15] In particular, we were interested in generating structural models related to an aristotype through a vacancy ordering involving a specific orbit of it (to obtain the wanted composition) and resulting in a desired local topology. To achieve this result several steps were needed:

(1) generation of all possible subgroups of the aristotype of a certain order,
(2) selection of a subset where the considered original orbit is split in two (a splitting into more orbits would contradict the symmetry principle),
(3) removal of one-half of the generated sites, corresponding to vacancies, and
(4) search for the structures containing the desired fragment. This final step was done using the original ToposPro algorithm of searching for a finite fragment in an infinite periodic net.

A step by step description of this procedure applied to the 2:1:6 family of structures is available in the Supporting Information.

2.4. Electronic Structure Calculations. The electronic band structure of $La_2Zn_{1-x}Ge_6$ (x = 0, idealized model corresponding to the stoichiometry 2:1:6) was calculated by means of the self-consistent, tight-binding, linear-muffin-tin-orbital method using the Stuttgart TB-LMTO-ASA 4.7 program[25] in the local density (LDA) and the atomic-spheres approximations (ASA) in the framework of the DFT method. Two empty spheres were introduced to satisfy the LMTO volume criterion (less than 10%; their positions were deduced by the automatic procedure implemented in the code). The average ASA radii for the constituents were as follows: La = 2.13 Å, Ge = 1.42−1.52 Å, Zn = 1.49 Å, empty spheres of ca. 1.04 Å both.

The basis sets included 6s, (6p), 5d, and 4f orbitals for La, 4s, 4p, and 3d orbitals for Zn, and 4s, 4p, and (4d) orbitals for Ge with orbitals in parentheses being downfolded.[26]

The k-space integrations were done using an improved tetrahedron method[27] with 365 irreducible k-points mesh in the first Brillouin zone. The energies and crystal orbital Hamilton populations (COHP) convergence with respect to the number of k points was checked in all calculations. The density of states (DOS), (COHP) curves,[26] and integrated COHP values (iCOHPs) were also calculated in order to evaluate orbital interactions. Plots of DOS and COHP curves were generated using wxDragon.[28]

3. RESULTS AND DISCUSSION

3.1. Crystal Structure Determination of $R_2Zn_{1-x}Ge_6$ (La, Ce, Nd, Gd, Tb, Dy) Germanides. Cell indexation was straightforward for crystals with R = La, Ce, Nd, and Tb (crystals I−III and V), giving an orthorhombic *C*-centered cell ($h + k = 2n$ reflections were observed). The analysis of systematic extinctions suggested as possible space groups *Cc*2*e* (No. 41) and *Cmce* (No. 64). The same, almost complete, structural model was obtained in a few iteration cycles by applying the charge-flipping algorithm implemented in *JANA2006*.[29] In this model the rare-earth atoms are situated in a 16*g* general site, while the other six positions were accidentally assigned to the lighter elements: in fact, the very similar X-ray scattering powers of Ge and Zn (which are only $2e^-$ different) make it difficult to distinguish between them. In any case the *oS*72 Pearson symbol is associated with this model. The final structure was then obtained by distributing Ge and Zn among the appropriate sites, taking into account both the measured compositions and previous knowledge on similar compounds, such as La_2MgGe_6[4] and Dy_2PdGe_6.[18] At this point it became clear that the La-, Ce-, Nd-, and Tb-containing compounds are isopointal with the $Ce_2(Ga_{0.1}Ge_{0.9})_7$ prototype.

Further structure refinements were carried out by full-matrix least-squares methods on $|F^2|$ using the SHELX programs[30] as implemented in WinGX.[31] The anisotropically refined R_2ZnGe_6 models showed acceptable residuals and flat difference Fourier maps. An unusual value of Zn 8*f* site anisotropic displacement parameter (ADP) was found for Nd_2ZnGe_6: for this reason its occupancy factor (SOF) was left to vary in further cycles, converging to ca. 0.85 and leading to even lower residuals and homogeneous ADP values for all species. At this point SOFs of all species were checked for deficiency, obtaining nevertheless values very close to unity. The same procedure was applied to the Tb analogue, converging to ca. 0.56 and to La and Ce compounds, giving a less pronounced Zn deficiency along with better residuals.

DOI: 10.1021/ic5030313
Inorg. Chem. 2015, 54, 2411−2424

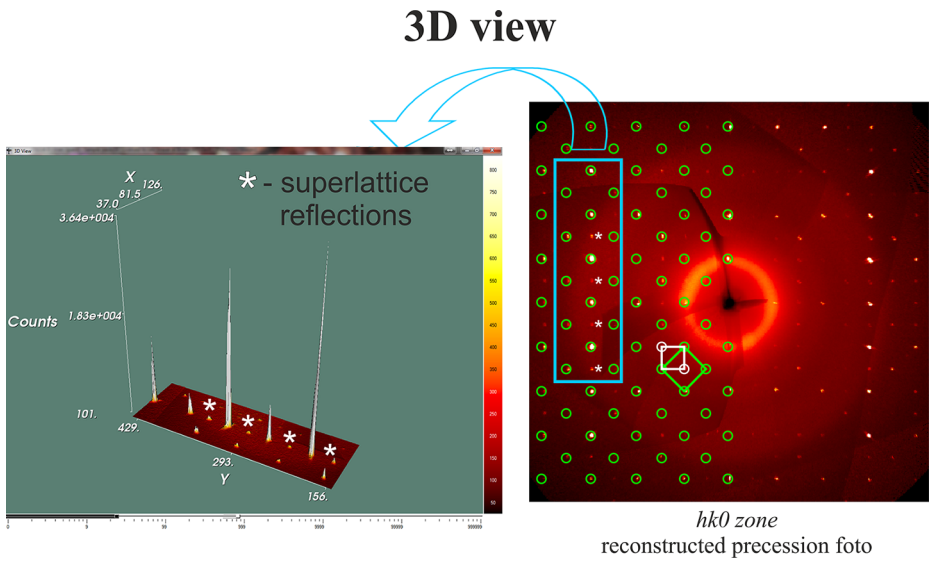

Figure 1. Observed intensity profiles for the *hk*0 zone demonstrating the presence of weak super-reflections. The reciprocal lattice corresponding to the *C*-centered monoclinic cell is shown in green; the reciprocal lattice of the monoclinic superstructure is shown in white; for clarity only some super-reflections are asterisked. The 3D image of the area marked in blue, highlighting the difference of peaks intensities, is also shown (left).

La_2AlGe_6-*mS*36
C 1 2/*m* 1
k2
1/4, 1/4, 0
Dy_2ZnGe_6-*mP*36
P 1 2_1/*m* 1
(calculated)

La:8*j*	Ge1:8*j*	Ge2:4*i*	Ge3:4*i*	Ge4:4*i*	Ge5:4*i*	Al:4*i*
1	1	*m*	*m*	*m*	*m*	*m*
0.085	0.278	0.07	0.986	0.146	0.140	0.300
0.248	0.213	0	1/2	0	1/2	1/2
0.336	0.113	0.112	0.113	0.564	0.580	0.195

Dy1:4*f*	Dy2:4*f*	Ge1:4*f*	Ge2:4*f*	Ge3:2*e*	Ge4:2*e*	Ge5:2*e*	Ge6:2*e*	Ge7:2*e*	Ge8:2*e*	Ge9:2*e*	Ge10:2*e*	Zn2:2*e*	Zn1:2*e*
1	1	1	1	*m*	*m*	*m*	*m*	*m*	*m*	*m*	*m*	*m*	*m*
0.335	0.835	0.538	0.038	0.320	0.820	0.237	0.736	0.396	0.896	0.390	0.890	0.550	0.050
0.498	0.998	0.463	0.963	1/4	3/4	3/4	1/4	1/4	3/4	3/4	1/4	3/4	1/4
0.336	0.336	0.113	0.113	0.112	0.112	0.113	0.113	0.564	0.564	0.580	0.580	0.195	0.195

$Dy_2Zn_{1-x}Ge_6$-*mP*34
P 1 2_1/*m* 1
(refined)

Dy1:4*f*	Dy2:4*f*	Ge1:4*f*	Ge2:4*f*	Ge3:2*e*	Ge4:2*e*	Ge5:2*e*	Ge6:2*e*	Ge7:2*e*	Ge8:2*e*	Ge9:2*e*	Ge10:2*e*	□/Zn2:2*e*	Zn1:2*e*
1	1	1	1	*m*	*m*	*m*	*m*	*m*	*m*	*m*	*m*	*m*	*m*
0.334	0.834	0.529	0.029	0.322	0.791	0.270	0.734	0.400	0.892	0.393	0.891	0.550	0.050
0.498	0.002	0.491	0.960	1/4	3/4	3/4	1/4	1/4	3/4	3/4	1/4	3/4	1/4
0.336	0.336	0.119	0.115	0.115	0.122	0.122	0.114	0.580	0.562	0.582	0.585	0.203	0.201

Figure 2. Group−subgroup relation in the *Bärnighausen* formalism for the *mS*36-La_2AlGe_6 and *mP*36-2-$Dy_2Zn_{1-x}Ge_6$ structural models. The type and order of the symmetry reduction and the evolution of the atomic parameters are shown.

The structure solution of $Gd_2Zn_{1-x}Ge_6$ (*crystal IV*) deserves a separate description. Despite the very good quality of the crystal, the indexation of the ca. 650 reflections selected from the complete collected data set was not unambiguous. In fact, the difference vectors and fast Fourier transform algorithms inside *APEX2*[23] suggested two different unit cells with very close score values: a *C*-orthorhombic cell (a = 8.02 Å, b = 8.33 Å, c = 20.83 Å, V = 1393 Å^3) and a *P*-monoclinic cell (a = 8.04 Å, b = 8.36 Å, c = 10.64 Å, β = 100.91°, V = 703 Å^3). After refinement both cells give very similar deviation histograms (see the Supporting Information), so that further integration was done for both cells independently. The analysis of the reflection conditions with *XPREP*[23] showed that the monoclinic choice was not compatible with any space group; instead, the orthorhombic one leads to the *Cmce* space group. The structural model was refined analogously to *crystals I*−*III* and *V*, giving for the Zn site a SOF ≈ 0.64.

In the case of the Dy crystal (*crystal VI*) a routine analysis of the obtained data set suggested a *C*-centered monoclinic cell (a = 7.96 Å, b = 8.25 Å, c = 10.53 Å, β = 100.9°). No systematic absences associated with symmetry elements were found, so structure solution was attempted in the *C*2/*m* space group, giving an adequate structural model (*JANA2006*) with excellent residuals (*SHELX*). This *mS*36 model is isopointal with the monoclinic La_2AlGe_6 prototype, showing a pronounced Zn deficiency (site 4*i*, SOF = 0.49). Occupancy factors values close to 1/2, 1/3, 1/4, etc., are often warning signs of a more chemically sound superstructure, where the atom distribution is better modeled by a higher number of sites, resulting from symmetry reduction.[4−6,10] This is the reason why a more careful analysis of the reciprocal diffraction lattice was performed. In fact, numerous weak super-reflections were clearly discerned (as an example, see the reconstructed precession photo in Figure 1).

DOI: 10.1021/ic5030313
Inorg. Chem. 2015, 54, 2411−2424

Table 3. Atomic Coordinates Standardized by Structure Tidy[33] and Equivalent Isotropic Displacement Parameters (Å^2) for the Studied Single Crystals

$R_2Zn_{1-x}Ge_6$ (orthorhombic)						
atom (site)	atomic params	R = La	R = Ce	R = Nd	R = Gd	R = Tb
R (16*g*)	*x*/*a*	0.25120(4)	0.25116(4)	0.25136(3)	0.25110(5)	0.25097(3)
	y/*b*	0.37387(5)	0.37387(4)	0.37386(3)	0.3748(3)	0.37479(8)
	z/*c*	0.08313(2)	0.08289(2)	0.08272(2)	0.08230(2)	0.08211(2)
	U_{eq} (Å^2)	0.00563(16)	0.0029(2)	0.00408(10)	0.00723(15)	0.00545(9)
Ge1 (8*f*)	*x*/*a*	0	0	0	0	0
	y/*b*	0.12111(14)	0.12030(13)	0.11999(10)	0.1210(6)	0.1212(2)
	z/*c*	0.46054(5)	0.45950(7)	0.45873(4)	0.45838(7)	0.45809(4)
	U_{eq} (Å^2)	0.0089(2)	0.0059(3)	0.00636(16)	0.0095(3)	0.00784(18)
Ge2 (8*f*)	*x*/*a*	0	0	0	0	0
	y/*b*	0.33397(14)	0.33512(18)	0.33727(11)	0.3423(3)	0.3462(2)
	z/*c*	0.30537(5)	0.30615(6)	0.30673(4)	0.30828(9)	0.30874(6)
	U_{eq} (Å^2)	0.0097(3)	0.0086(3)	0.01048(18)	0.0199(7)	0.0223(4)
Ge3 (16*g*)	*x*/*a*	0.28581(9)	0.28463(13)	0.28254(7)	0.27698(15)	0.27563(11)
	y/*b*	0.12443(10)	0.12403(9)	0.12436(7)	0.1250(4)	0.12478(16)
	z/*c*	0.19457(3)	0.19400(4)	0.19338(3)	0.19234(5)	0.19179(3)
	U_{eq} (Å^2)	0.0096(2)	0.0082(3)	0.00967(14)	0.0197(3)	0.01880(18)
Ge4 (8*f*)	*x*/*a*	0	0	0	0	0
	y/*b*	0.12902(14)	0.12951(13)	0.13011(10)	0.1289(6)	0.1288(2)
	z/*c*	0.03138(5)	0.03118(7)	0.03132(4)	0.03368(8)	0.03422(5)
	U_{eq} (Å^2)	0.0080(2)	0.0056(3)	0.00644(16)	0.0126(3)	0.01191(19)
Ge5 (8*f*)	*x*/*a*	0	0	0	0	0
	y/*b*	0.41456(14)	0.41288(19)	0.41174(11)	0.4052(4)	0.4053(2)
	z/*c*	0.19427(5)	0.19367(6)	0.19307(4)	0.19191(9)	0.19116(6)
	U_{eq} (Å^2)	0.0100(3)	0.0090(3)	0.01055(18)	0.0241(8)	0.0201(3)
Zn (8*f*)	*x*/*a*	0	0	0	0	0
	y/*b*	0.12385(16)	0.12395(16)	0.12413(13)	0.1246(4)	0.1251(3)
	z/*c*	0.15024(6)	0.14899(7)	0.14842(5)	0.14844(12)	0.14852(8)
	U_{eq} (Å^2)	0.0086(4)	0.0072(5)	0.0070(3)	0.0106(8)	0.0088(5)
	SOF ≠ 1	0.937(6)	0.911(9)	0.844(5)	0.636(6)	0.563(6)

$Dy_2Zn_{1-x}Ge_6$ (monoclinic)						
atom	site	SOF	*x*/*a*	*y*/*b*	*z*/*c*	U_{eq} (Å^2)
Dy1	4*f*		0.16585(3)	0.50010(3)	0.66415(3)	0.00482(9)
Dy2	4*f*		0.33395(3)	0.00186(3)	0.33642(3)	0.00476(9)
Ge1	2*e*		0.89134(11)	1/4	0.58539(9)	0.00653(17)
Ge2	2*e*		0.72997(14)	1/4	0.87735(9)	0.0141(2)
Ge3	2*e*		0.40029(11)	1/4	0.57967(10)	0.00948(18)
Ge4	4*f*		0.02863(9)	0.53853(10)	0.11485(6)	0.01302(16)
Ge5	2*e*		0.32226(14)	1/4	0.11487(9)	0.0138(2)
Ge6	2*e*		0.10813(11)	1/4	0.43809(9)	0.00821(18)
Ge7	2*e*		0.60605(11)	1/4	0.41784(9)	0.00695(17)
Ge8	2*e*		0.20860(14)	1/4	0.87760(9)	0.0141(2)
Ge9	4*f*		0.52973(9)	0.00910(9)	0.11951(7)	0.01312(16)
Ge10	2*e*		0.73492(14)	1/4	0.11474(9)	0.0140(2)
Zn1	2*e*	0.822(4)	0.05023(15)	1/4	0.20193(12)	0.0077(3)
Zn2	2*e*	0.178(4)	0.4492(8)	1/4	0.7967(6)	0.0137(16)

Considering these weak super-reflections, indexation results in a primitive monoclinic cell with the same lattice parameters. A new model was found by *JANA2006* in the $P2_1/m$ (No. 11) space group, containing 13 crystallographic positions: for analogy with other 2:1:6 compounds 2 of them were assigned to Dy, 10 to Ge, and 1 to Zn atoms. Nonetheless, one additional prominent peak maximum at 0.45, 1/4, 0.80 was found on the difference Fourier map. This peak was associated with an additional Zn position, but considering the distances to the closest neighbors the SOFs of Zn sites were left to vary. As the sum of SOFs for them was close to unity, this condition was constrained to hold up in further cycles of refinement (obtaining a SOFs ratio of 0.82(Zn1):0.18(Zn2)). In the final *mP*36-2 model containing 14 positions, all atoms were refined anisotropically except for the Zn1−Zn2 couple; their ADPs were constrained to be identical. The refinement converged at R1 = 0.0268, *w*R2 = 0.0683, and GOF = 0.98 complemented by a flat difference Fourier map. The goodness of the accepted model is also highlighted by the less pronounced anisotropic displacement parameters for Ge atoms closest to Zn positions and by a more homogeneous distribution of all ADPs.

Frequently, a superstructure requiring an enlargement of the unit cell is *klassengleiche* group−subgroup related to the structural model assumed initially, which is why such a relation

DOI: 10.1021/ic5030313
Inorg. Chem. 2015, 54, 2411−2424

was looked for between the *mS*36-La_2AlGe_6 and *mP*34-$Dy_2Zn_{1-x}Ge_6$ structural models. From the *Bärnighausen* chart shown in Figure 2 it can be noted that refined atomic coordinates of the major part of observed atom positions ($Dy_2Zn_{1-x}Ge_6$-*mP*34) fit very well with those obtained from corresponding sites splitting ($Dy_2Zn_{1-x}Ge_6$-*mP*36); the 1/2 1/2 0 translation vector vanishes, leaving more degrees of freedom for a shift of Ge species and causes the formation of two independent Zn sites (having different SOFs in the final model). These features can be interpreted in terms of a vacancy ordering phenomenon, which will be discussed in more detail in the following paragraphs.

3.2. Microstructure, Phase Analysis, and Crystal Structure Description of the $R_2Zn_{1-x}Ge_6$ Phases. Phases detected in ternary samples of nominal composition $R_{22.2}M_{11.1}Ge_{66.7}$ are listed in the Supporting Information, together with their measured compositions and lattice parameters. All examined alloys are multiphase: for all rare-earth metals, except for Er and Tm, the main phase is a ternary compound where the ratio between elements approaches the 2:1:6 stoichiometry. Common secondary phases are Ge (R = La, Sm, Gd, Dy–Tm), RGe_{2-x} (R = La–Nd, Sm, Tm), $R_2Zn_3Ge_6$ (R = La–Pr, Sm, Gd–Ho), $R_4Zn_5Ge_6$ (R = Er, Tm), and RZn_xGe_2 (R = Tb–Er). This last series of novel compounds is currently under investigation in our research group. A new ternary compound was also detected for Sm of composition ~$Sm_{27}Zn_6Ge_{67}$. Selected microphotographs of the characterized samples are also shown in the Supporting Information. Along the 2:1:6 series, the measured Zn content smoothly decreases on increasing the R atomic number, passing from 11.0 atom % (for La) to 5.7 atom % (for Ho); the general formula $R_2Zn_{1-x}Ge_6$ conveniently accounts for this feature.

The X-ray diffraction powder patterns can be satisfactorily interpreted assuming the $R_2Zn_{1-x}Ge_6$ compounds belonging to any of the three structural models reported in the literature (see Introduction), whose crystal spaces are indeed characterized by the same distribution of the rare-earth metal atoms and most of the lighter constituents. The small differences between these models are hardly distinguishable in the theoretical powder patterns and not visible at all in the experimental patterns of multiphase samples, where strong peak overlapping occurs.

For these reasons single-crystal X-ray diffraction was performed on several samples along the series (R = La, Ce, Nd, Gd, Tb, Dy) with the aim to find the correct structural model(s) and shed more light on the Zn deficiency. To our knowledge, such behavior was not previously detected in the R_2MGe_6 family; instead, it was observed for other R–Zn–Ge series of compounds, especially for heavy rare-earth metals.[32]

Considering the single crystals (see section 3.1) and powder X-ray diffraction analysis results together with the behavior regularities along the R series it was concluded that the orthorhombic structure (*oS*72-$Ce_2(Ga_{0.1}Ge_{0.9})_7$) is realized for R = La–Nd, Sm, Gd–Tb and the monoclinic one (*mP*34-$Dy_2Zn_{1-x}Ge_6$) for the Dy analogue. Unfortunately, it was not possible to isolate a good quality $Ho_2Zn_{1-x}Ge_6$ single crystal; nevertheless, we are inclined to believe that the latter is also monoclinic since the structure changed passing from Tb to Dy.

The established structural models (see Table 3) support the Zn deficiency (and its trend within the series) suggested by the EDXS characterization. In fact, in both the orthorhombic and the monoclinic compounds the SOFs of the Zn sites are <1, leading to a smooth decrease of the Zn content along the R series. This trend is plotted in Figure 3, where only the *x* values

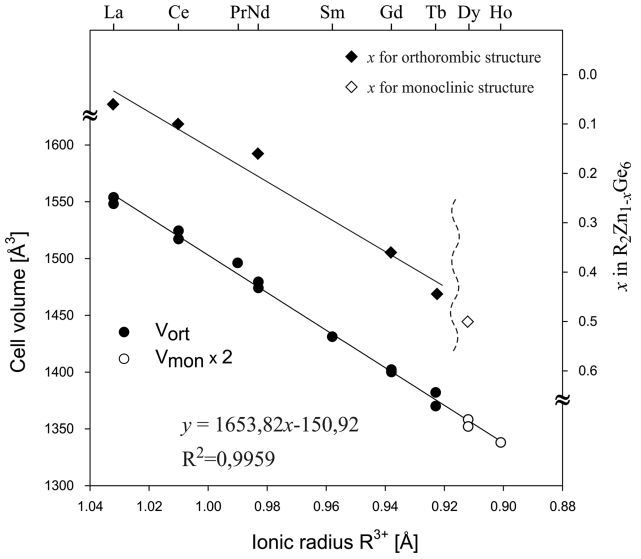

Figure 3. Normalized cell volumes (both from single-crystal and powder XRD data) and deficiency (*x*) of $R_2Zn_{1-x}Ge_6$ compounds as a function of the R^{3+} ionic radius.

obtained from single crystals were considered. In the same figure the cell volume linearly decreasing along the series is also shown; in order to compare the different structures, the monoclinic cell volume was doubled (in this way the same number of atoms was taken into account).

From the interatomic distances analysis of all the compounds (see Table 4 and the Supporting Information) it is possible to highlight the presence of two types of covalently bonded Ge fragments, shown in Figure 4: 2D zigzag chains formed by two-bonded (2b-) Ge atoms and 3D corrugated layers formed by three-bonded (3b-) Ge atoms. Within these fragments the Ge–Ge distances range from ca. 2.46 to 2.63 Å and are not strongly affected by the lanthanide contraction. These motifs, common to the orthorhombic and monoclinic structures, are joined by Zn–Ge bonds to form a framework whose channels are filled by the bigger R atoms. Each Zn atom is connected to five Ge atoms (dotted lines in Figure 4) with distances comparable to their atomic radii sum: the shortest of them corresponds to the links between Zn and the 2D germanium zigzag chains. Passing from La to Tb this contact regularly shrinks, as a consequence of both the lanthanide contraction and the increasing Zn deficiency effects. A non-negligible contribution of the Zn deficiency can be revealed by comparing the trend of Zn–Ge distances in the analogous framework in $R_2Zn_3Ge_6$ compounds (R = La–Nd).[11] In the monoclinic $Dy_2Zn_{1-x}Ge_6$ compound (Figure 4b) the Ge covalent fragments are linked in a slightly different manner, and the Zn linkers occupy two distinct sites characterized by very different SOFs: the Zn–Ge link distance for the higher SOF Zn atoms is on the order of atomic sum radii; instead, that for the remaining Zn species (with very low SOF) is physically unreasonable.

It is appropriate to underline here that also the germanium 3D covalent fragments undergo a significant change when examining the whole series of compounds. These fragments are infinite, corrugated layers composed of interconnected squares, and they can be viewed also as distorted α-Po motifs (see Introduction). Their distortion degree, which can be qualitatively evaluated by the Ge–Ge–Ge obtuse angle (α) indicated in Figure 4a, decreases along with the zinc content, so the less distortion found in the orthorhombic compounds

DOI: 10.1021/ic5030313
Inorg. Chem. 2015, 54, 2411–2424

Table 4. Interatomic Distances and Integrated Crystal Orbital Hamilton Populations (−*i*COHP, eV per bond per cell) at E_F for the Strongest Contacts within the First Coordination Spheres in La_2ZnGe_6

central atom	adjacent atoms	*d* (Å)	−*i*COHP	central atom	adjacent atoms	*d* (Å)	−*i*COHP
La	Ge1	3.144(1)	1.11	Ge3(3b-)	Ge3	2.462(1)	2.75
	Ge1	3.159(1)	1.08		Ge2	2.551(1)	1.91
	Ge3	3.177(1)	0.97		Ge5	2.553(1)	1.91
	Ge3	3.185(1)	0.96		Zn	2.671(1)	1.27
	Ge4	3.187(1)	1.04		La	3.177(1)	0.97
	Ge4	3.228(1)	0.96		La	3.185(1)	0.96
	Ge2	3.250(1)	0.86	Ge4(2b-)	Ge4	2.527(2)	2.33
	Ge5	3.259(1)	0.85		Zn	2.554(2)	1.44
	Ge4	3.282(1)	0.85		Ge1	2.569(2)	2.13
	Zn	3.329(1)	0.37		2La	3.187(1)	1.04
	Zn	3.343(1)	0.37		2La	3.228(1)	0.96
	Ge1	3.427(1)	0.67		2La	3.282(1)	0.85
Ge1(2b-)	Ge4	2.569(2)	2.13	Ge5(3b-)	Ge2	2.478(2)	2.69
	Ge1	2.627(2)	1.94		2Ge3	2.553(1)	1.91
	2La	3.144(1)	1.11		Zn	2.587(2)	1.43
	2La	3.159(1)	1.08		2La	3.259(1)	0.85
	2La	3.427(1)	0.67	Zn	Ge4	2.554(2)	1.44
Ge2(3b-)	Ge5	2.478(2)	2.69		Ge2	2.584(2)	1.43
	2Ge3	2.551(1)	1.91		Ge5	2.587(2)	1.43
	Zn	2.584(2)	1.43		2Ge3	2.671(1)	1.27
	2La	3.250(1)	0.86		2La	3.329(1)	0.37
					2La	3.343(1)	0.37

occurs for the Tb analogue, where $\alpha \approx 100°$ and SOF(Zn) = 0.56. For the monoclinic compound the distortion locally depends on the SOF value of the capping Zn atom, being more pronounced for the Zn highly occupied 2*e* site (see insert in Figure 4b). A similar distortion was observed for $RAl_{1-x}Ge_2$[5] and $RFe_{1-x}Ge_2$[6] compounds in planar Ge networks capped by Al or Fe.

An ideal α-Po layer formed by Ge atoms (with all Ge−Ge−Ge solid angles equal to 90°) exists in the binary compound $TmGe_3$, where these layers are directly linked to Ge−Ge zigzag chains by Ge−Ge contacts.[9]

From previous considerations it is clear that the Zn content is a key factor for the structural changes along this series.

3.3. R_2MGe_6 Family in Terms of Vacancy Ordering. It often happens that very similar crystal structures (also with related metric conditions) are group−subgroup related: it is not the case of *oS*72-$Ce_2(Ga_{0.1}Ge_{0.9})_7$ and *mS*36-La_2AlGe_6. An alternative relation was looked for through a common supergroup, but no aristotype was found for which the Wyckoff sites split generates the two structural models under study. Nevertheless, they were described by Zhao et al.[34] as vacancy variants of the orthorhombic $SmNiGe_3$ type. Adopting this point of view we decided to start from this aristotype and reduce its symmetry, considering vacancies as a part of the symmetry criteria. Results are summarized in Figure 5 in the form of a *Bärnighausen* tree (the corresponding evolutions of atomic parameters are provided in the Supporting Information). All three *oS*72, *mS*36, and *mP*36-2 structures find their own place inside this two-branched tree. The *oS*72 stays on the orthorhombic branch, resulting from two successive k2 reduction steps. Referring to the atomic species, the original orbit of the Ni atoms splits in two subsets: one is occupied by Zn atoms, and the other remains vacant.

The monoclinic branch starts from the *mS*36 model, resulting after two successive reduction steps, of t2 and k2 type. Also, in this case the original 4*i* Ni site splits into two 4*i* sites, one of which is vacant. At this point, the two 2:1:6 models situated at the same level of hierarchy could be called "isomers". Their different vacancy (empty circles) distribution is shown in Figure 6a, where the trace of the aristotype unit cell is evidenced in red. In terms of constituting structural fragments, one can observe that for both isomers one-half of the bridging atoms entails a similar distortion of the 3D corrugated Ge layers (see Figure 6b).

The *oS*72 and *mS*36 models can be the starting points of a further *klassengleiche* reduction, leading to 4:1:12 isomers characterized by an even smaller number of bridging atoms. The *mP*36-2 model found for the $Dy_2Zn_{1-x}Ge_6$ phase is one of them on the monoclinic branch. The symmetry reduction between *mS*36 and *mP*36-2 was already described in section 3.1 while discussing how the correct structural model was discerned; generalized schemes like this are helpful in solving new structures, providing a finite number of models to test.[15]

In order to check if other 2:1:6 isomers may exist, deriving from the $SmNiGe_3$ aristotype and characterized by the same symmetry criteria, the ToposPro software was applied using the batch of algorithms described in section 2.3 and in the Supporting Information. Only the subgroups of fourth order were considered. At the end of this procedure only the two isomers already described were found. The same procedure could be applied to find all 4:1:12 isomers starting from each of the 2:1:6 models; however, no orthorhombic 4:1:12 isomers were found characterized by the same local topology as the idealized monoclinic $Dy_2Zn_{1-x}Ge_6$ (x = 0.5, only one Zn site fully occupied, composition Dy_4ZnGe_{12}).

At this point it is clear that the vacancy ordering criterion has been a successful approach to find a general scheme including all of the structures found. On the other hand, the structural and chemical role of vacancy phenomena has been described for other germanides[4,35−37] and different classes of compounds, such as intermetallic clathrates,[38,39] γ-brasses,[40,41] and superconducting oxides.[14]

DOI: 10.1021/ic5030313
Inorg. Chem. 2015, 54, 2411−2424

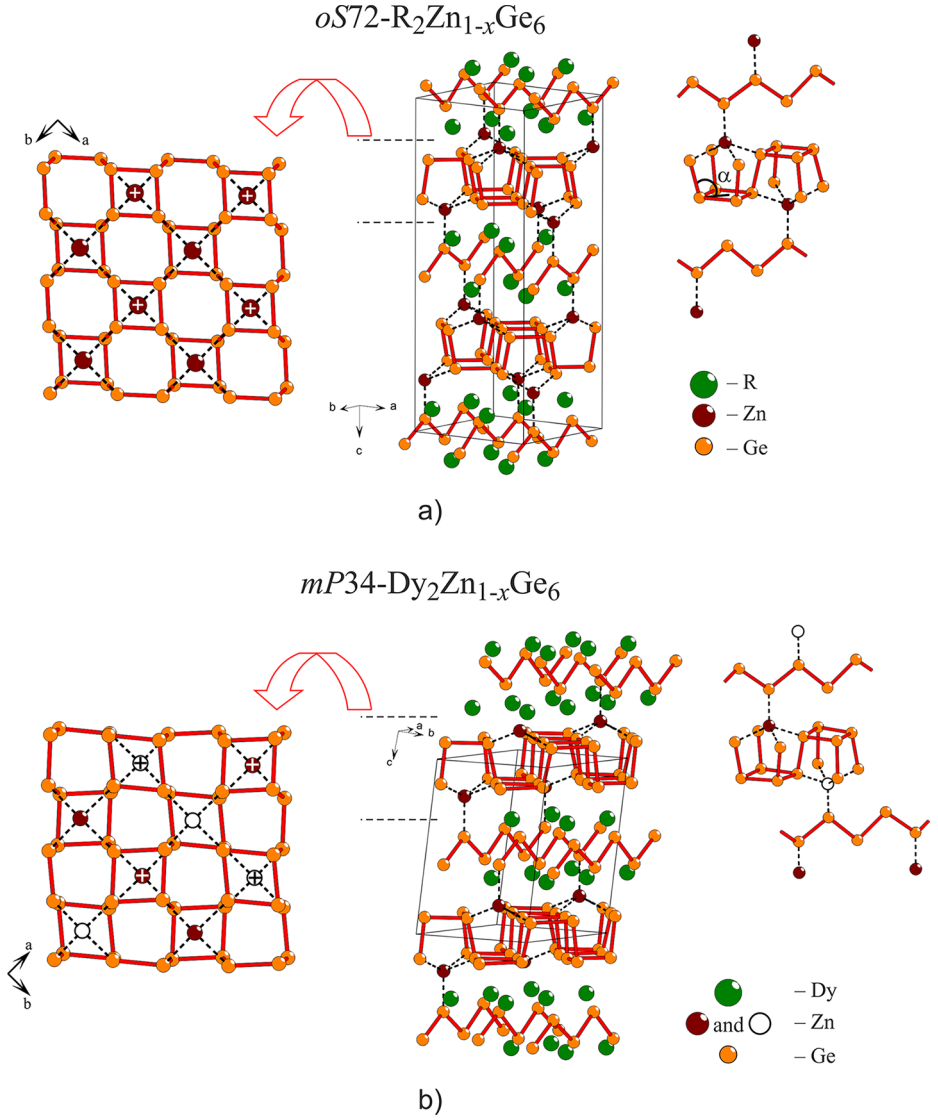

Figure 4. Representation of the crystal structures of (a) $R_2Zn_{1-x}Ge_6$ (*oS*72) and (b) $Dy_2Zn_{1-x}Ge_6$ (*mP*34) as composed of Zn−Ge networks sandwiched by R atoms (filled in green). Within this network the homocontacts Ge−Ge are shown in red; the heterocontacts Zn−Ge are black dotted lines. To highlight the different distortion degree of the 3b-Ge corrugated layers in these two structures, their projections along the *c* direction are shown in the left part of the figure (empty spheres represent Zn atoms with the smallest SOF, "+" indicates capping Zn atoms situated under the plane of image, remaining Zn atoms are located above it). The different spatial distribution/connection of the 2b-Ge "zigzag" chains with the 3b-Ge corrugated layers through the Zn linkers is shown to the right.

The proposed scheme based on vacancy ordering is complementary to the geometrical description of the same family of compounds in terms of linear intergrowth of topologically related fragments (of $BaAl_4$, AlB_2, and α-Po structure types). In particular, our approach describes also the compositional change of the $BaAl_4$-type slab, which is RX_4 for $SmNiGe_3$, $R\square X_3$ for the 2:1:6 isomers, and $R\square_2X_2$ for Dy_4ZnGe_{12} (R = bigger atom, X = smaller atom(s)). Thus, it allows us to relate structures belonging to different homological series.[42,43] Nevertheless, the linear intergrowth representation of the $SmNiGe_3$ and the 2:1:6 derivatives is useful to visualize the subtle differences between these structures (see Supporting Information).

3.4. $R_2Zn_3Ge_6$ Series of Compounds. Compounds of formula $R_2Zn_3Ge_6$ and crystal structure *oS*44-$La_2Zn_3Ge_6$, known from the literature for R = La−Nd,[11] were found as secondary phases in many samples synthesized in this work (see the Supporting Information). Therefore, it was possible to confirm their existence and crystal structure for some light rare-earth metals and to extend the series to R = Sm, Gd−Ho. The powder diffraction patterns of our samples can be indexed assuming the *oS*44-$La_2Zn_3Ge_6$ structure model for these heavy rare-earth 2:3:6 analogues.

The calculated cell volumes are shown in Figure 7 as a function of the R^{3+} radius, together with literature data: a linear decreasing trend is obtained, in agreement with the lanthanide contraction phenomenon.

The *oS*44-$R_2Zn_3Ge_6$ structures were described by Salvador et al.[11] as composed from PbO-like ZnGe layers and $ZnGe_4$ layers, with R atoms embedded within. Here, we propose an alternative description from the linear intergrowth point of view, discerning three types of intergrown 2D fragments (Figure 8) of $BaAl_4$, $Ba\square Al_3$, and α-Po topology (their compositions are RZn_2Ge_2, $RZn\square Ge_2$, and Ge_2, respectively). This description highlights the similarity between the $R_2Zn_3Ge_6$ and the $R_2Zn_{1-x}Ge_6$ families, particularly the presence of similar

DOI: 10.1021/ic5030313
Inorg. Chem. 2015, 54, 2411−2424

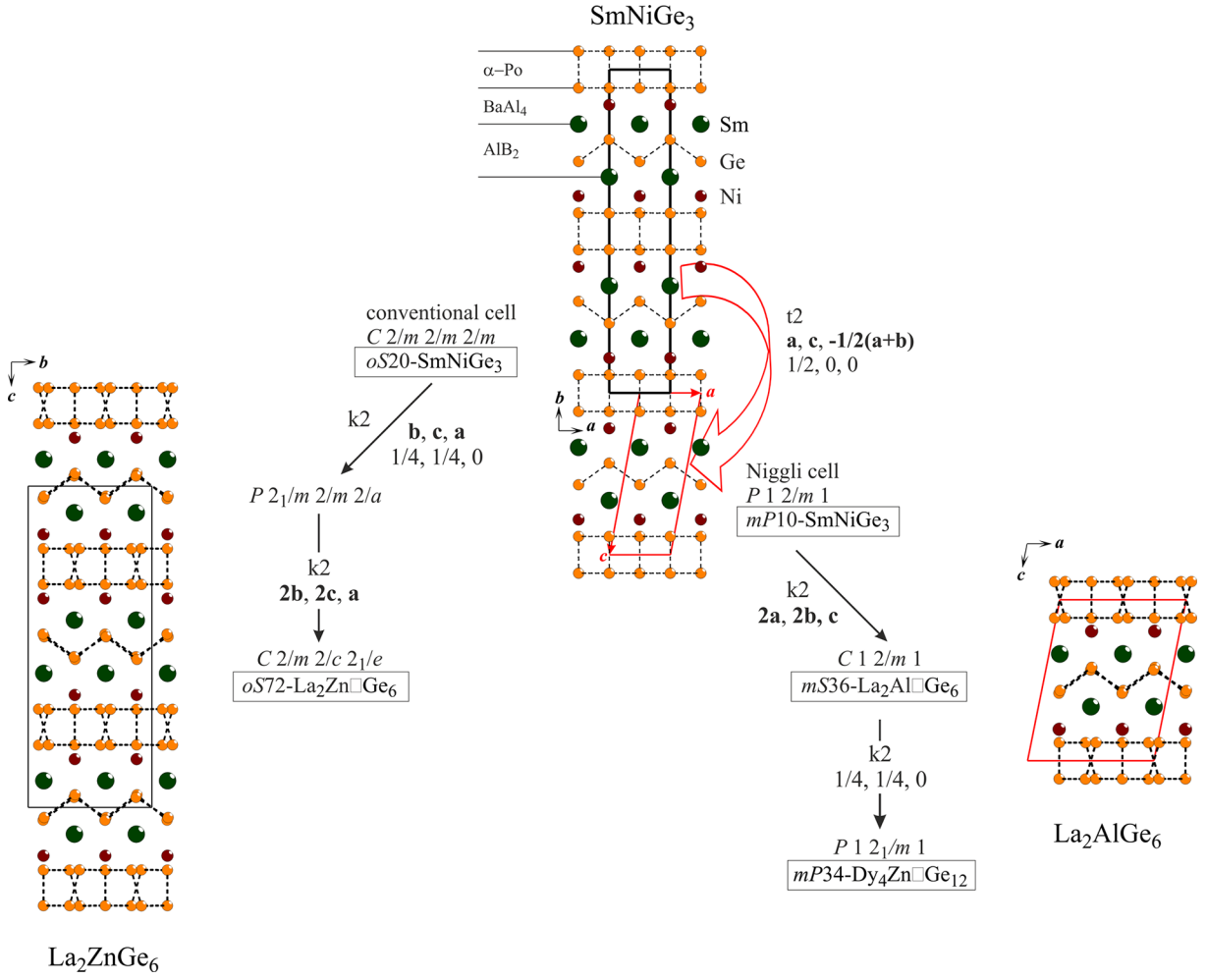

Figure 5. *Bärnighausen* tree relating the $SmNiGe_3$ aristotype and its orthorhombic and monoclinic vacancy variants. The type and indexes of the symmetry reductions are given.

3b-Ge-based corrugated layers capped by Zn atoms. Also, the interatomic distances within these fragments are very close for La representatives of the two series. For these reasons the vacancy ordering structural criterion was applied and proved to be valid also for the 2:3:6 series. The vacancy-free aristotype was found using the PSEUDO algorithm on the Bilbao server[44] after adding another Zn species in the appropriate position (4*c* site at 0, 0.348, 1/4). The obtained structure really exists, and it has only the *tI*24-$ScNi_2Si_3$ representative. Thus, the $R_2Zn_3\square Ge_6$ structure can be obtained from this aristotype reducing its symmetry in two steps: a *translationengleiche* (t2) decentering followed by a second-order *klassengleiche* transformation (k2), as represented in Figure 8 (left branch) in the form of a *Bärnighausen* tree. The corresponding evolution of atomic parameters is provided in the Supporting Information. It can be noted that this reduction does not contradict the symmetry principle (i.e., the number of Zn sites after splitting is minimal, only two). At this point, all 2:3:6 isomers can be generated from the $ScNi_2Si_3$ aristotype, applying the same ToposPro algorithms described for the 2:1:6 compounds. Also, in this case only two isomers were obtained: the already discussed $R_2Zn_3\square Ge_6$ (*oS*44, space group *Cmcm*) and the hypothetical "$R_2Zn_3\square Ge_6$" (*tI*88, space group $I4_1/amd$). The latter is represented in the right branch of Figure 8, and no real representatives of it are known to date. The linear intergrowth representation of $ScNi_2Si_3$ and its 2:3:6 derivatives is shown in the Supporting Information. The 2:3:6 isomers can become the starting points of further symmetry reductions (and vacancy concentration increase), leading to hypothetical 4:5:12 stoichiometries.

On the basis of this scheme one cannot exclude that even in the $R_2Zn_3Ge_6$ series vacancy ordering phenomena may exist, giving a general formula $R_2Zn_{3-x}Ge_6$ ($R_4Zn_5Ge_{12}$ for $x = 0.5$) and leading to crystal structures different from *oS*44 for some heavy rare-earth metals. Some experimental hints of this scenario already exist.

(1) The $R_2Zn_3Ge_6$ series extends up to R = Ho as the $R_2Zn_{1-x}Ge_6$ series.

(2) The EDXS measured compositions of $R_2Zn_3Ge_6$ show deviations from the ideal stoichiometry. The entity of this deviation and its trend along the R series (see the Supporting Information) are compatible with the $R_2Zn_{3-x}Ge_6$ hypothetical formula. In fact, the fraction of vacancies with respect to the overall number of atoms in the unit cell is smaller than for $R_2Zn_{1-x}Ge_6$. For example, the measured composition for R = Ho (24.8 atom % Zn; 56.2 atom % Ge) is closer to the hypothetical $Ho_4Zn_5Ge_{12}$ formula than to the $Ho_2Zn_3Ge_6$ stoichiometry.

X-ray single-crystal measurements would be necessary to confirm/discard this hypothesis. Selected structure models to

DOI: 10.1021/ic5030313
Inorg. Chem. 2015, 54, 2411−2424

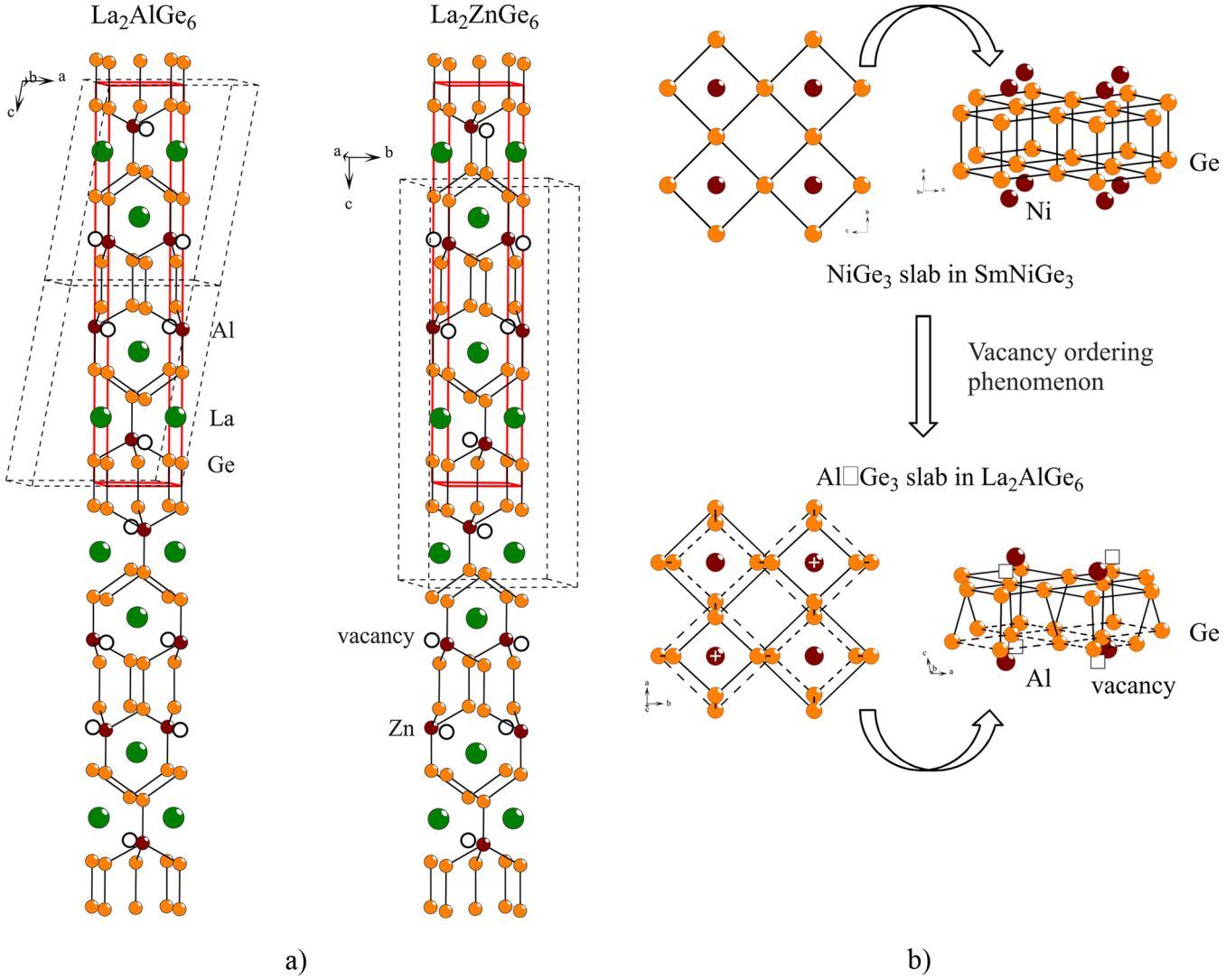

Figure 6. (a) Vacancy (empty circles) distribution in La_2ZnGe_6 (*oS*72) and La_2AlGe_6 (*mS*36) with respect to the $SmNiGe_3$ aristotype unit cell evidenced in red; (b) distortion of the 3b-Ge corrugated layer in $La_2Al\square Ge_6$ compared with that in $SmNiGe_3$.

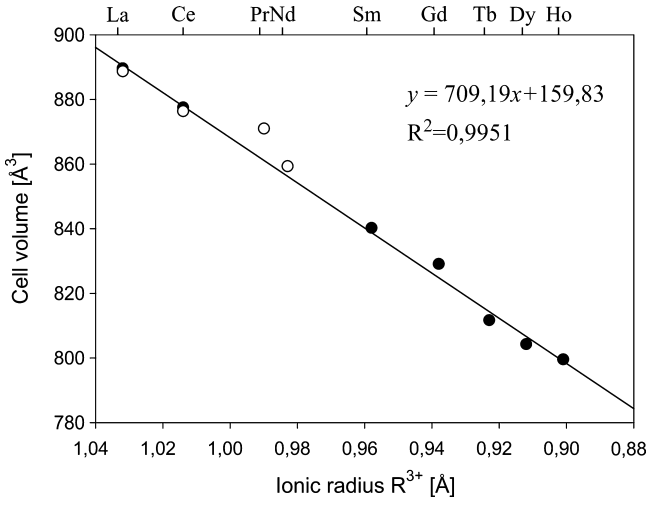

Figure 7. Cell volumes of $R_2Zn_3Ge_6$ compounds as a function of the R^{3+} ionic radius ((○) from ref 11; (●) this work).

test can be obtained extending the scheme of Figure 8 with further symmetry reduction based on a higher degree of vacancy ordering.

The $La_2Zn_3Ge_6$ compound was studied by Salvador et al.[11] also from the chemical bonding point of view. With the goal of comparing the chemistry of the polar 2:1:6 and 2:3:6 compounds, electronic structure calculations were performed on the La_2ZnGe_6 idealized model, and results are discussed in the next paragraph.

3.5. Electronic Structure Calculations for La_2ZnGe_6. The bonding in $R_2Zn_{1-x}Ge_6$ (x = 0, idealized models) can be initially addressed by the Zintl−Klemm concept.[45,46] Following this idea, the calculated valence electron concentration on Ge atoms, being <8 (VEC(Ge) = 5.3), suggests the presence of polyanionic network(s). The average number of Ge−Ge homocontacts is 8 − VEC(Ge) = 2.7, in agreement with the presence of two types of Ge fragments, with two and three homocontacts. Taking into account their ratio in the structure, the simplified ionic formula $(R^{3+})_2(Zn^{2+})(2b\text{-}Ge^{2-})_2(3b\text{-}Ge^{-})_4$ is obtained.

With the aim of investigating the chemical bonding within the 2:1:6 series, the electronic structure of La_2ZnGe_6 was

DOI: 10.1021/ic5030313
Inorg. Chem. 2015, 54, 2411−2424

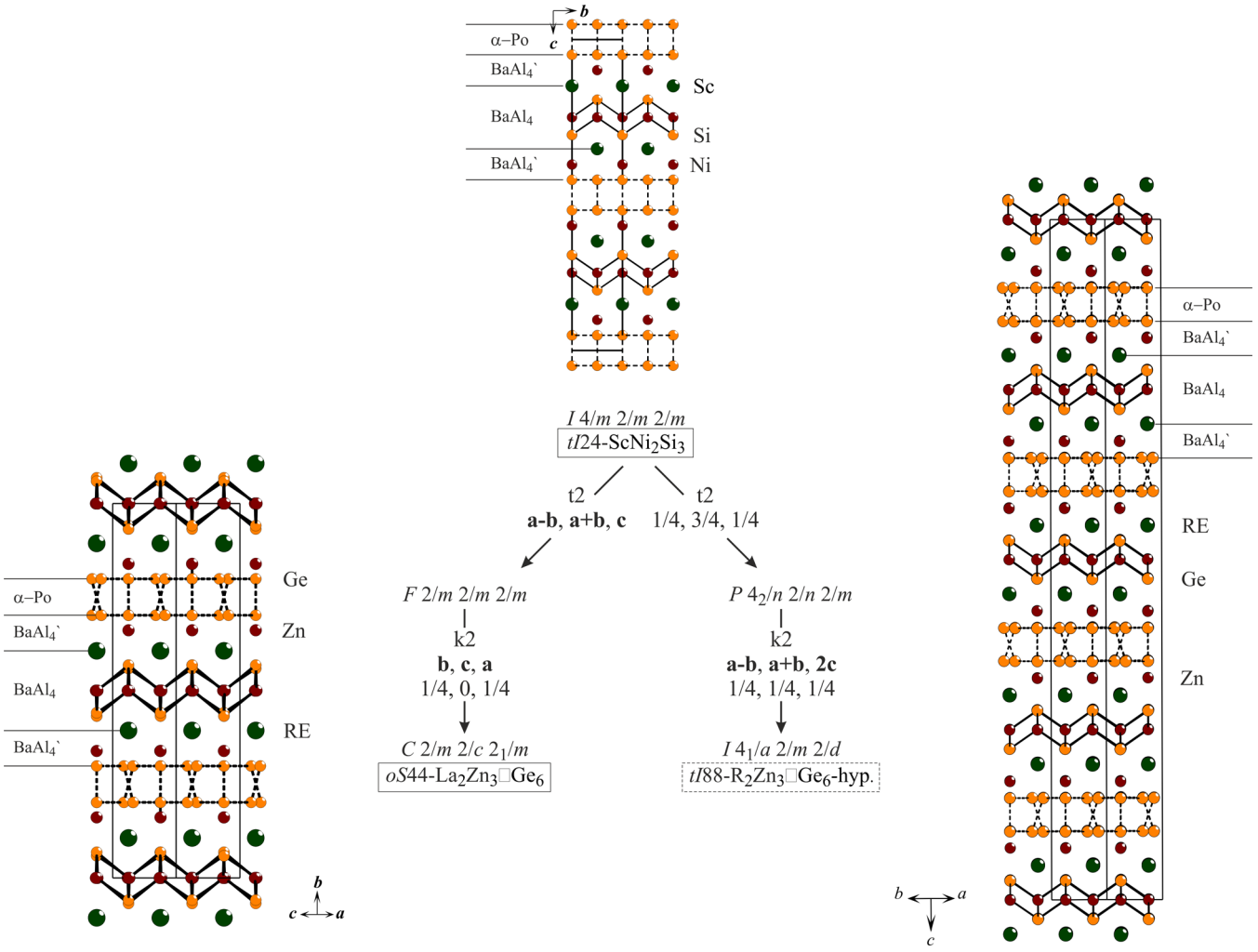

Figure 8. *Bärnighausen* tree relating the $ScNi_2Si_3$ aristotype and its orthorhombic and tetragonal vacancy variants. The type and indexes of the symmetry reductions are given.

computed by the TB-LMTO-ASA software. The La analogue was chosen for two reasons: it has no partially filled 4f orbitals, and its composition is very close to the idealized 2:1:6 stoichiometry.

The total and projected densities of states (DOS) of La_2ZnGe_6 are shown in Figure 9.

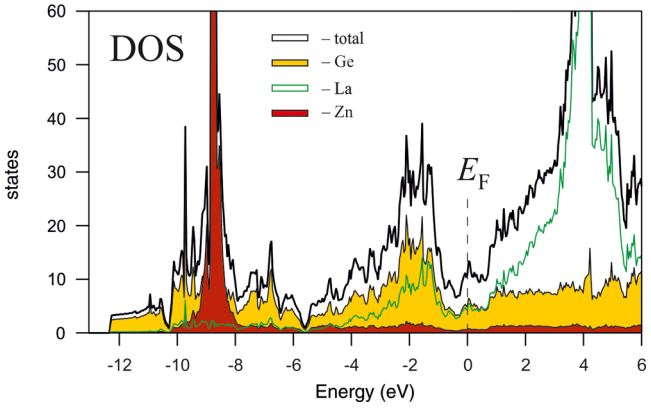

Figure 9. Total and projected DOS for La_2ZnGe_6 (E_F is set at 0 eV).

The DOS curve is characterized by a small number of states at the Fermi level, indicating a metallic character. Nevertheless, a minimum of the DOS (pseudogap) lies just below E_F.

The wide prominent peak from 3 to 5 eV in the conduction band is mainly due to the empty f La states.

The valence band (VB) of the DOS plot can be divided into two distinct regions: up to −6 eV and from −6 eV to E_F. The lower region is dominated by the filled d^{10} states of Zn atoms (prominent sharp peak between −9 and −8 eV). This feature was already observed for the structurally and chemically similar $R_2Zn_3Ge_6$[2] and $Ca_2Zn_3Sn_6$[47] compounds, where these states are regarded as "pseudo core states", so that Zn behaves as a "pseudo main group element". This is confirmed by the distribution of s and p states of Zn, spread over the region from −6 eV to E_F, where they overlap with s and p states of Ge. These features suggest a s−p-bonded $[ZnGe_6]^{\delta-}$ network, following the scenario proposed by Häussermann et al.[48] for a large number of binary and ternary polar intermetallics, including germanides.

A significant contribution of d states of La is observed just below the Fermi level, indicating that the La atoms do not transfer completely their valence electrons to the polyanionic network. These valence d states are hybridized with p states of Ge, suggesting strong La−Ge interactions, supported by the reciprocal arrangements and interatomic distances between

DOI: 10.1021/ic5030313
Inorg. Chem. 2015, 54, 2411−2424

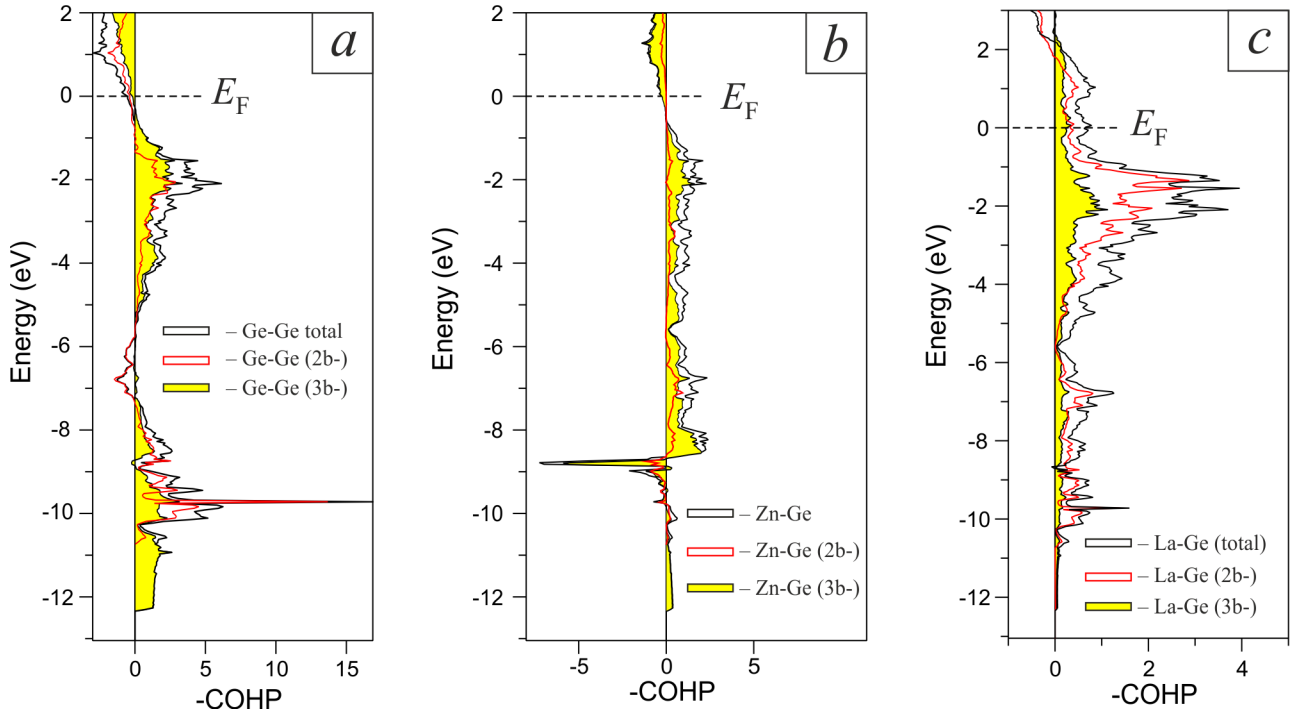

Figure 10. Crystal orbital Hamilton populations (−COHP) per bond for La_2ZnGe_6 from LMTO calculations: (a) Ge−Ge interactions; (b) Zn−Ge interactions; (c) La−Ge interactions.

these atoms in the crystal structure (see the presence of $GeLa_6$ trigonal prisms within the AlB_2-type slabs). The partial DOS curves relevant for this discussion are shown in the Supporting Information.

Further indications on bonding interactions and their strength can be taken from the COHP curves (shown in Figure 10) and their integrated values (−*i*COHP, listed in Table 4).

The Ge−Ge and Zn−Ge interactions change their character from bonding to antibonding type just below the Fermi level: similar features have been often interpreted in the literature as a qualitative indication that an ideal "electron tuning" would be achieved for a somewhat more electron poor model.[49,50] In fact, this is coherent with the real $La_2Zn_{1-x}Ge_6$ model, showing a small Zn deficiency, which indeed increases along the series. In the Ge−Ge COHP curves (Figure 10a) two different behaviors can be distinguished. The curve corresponding to the Ge−Ge (2b-) forming zigzag chains shows a small antibonding region below E_F (around −7 eV) corresponding to π^* states. An analogous interpretation was proposed for topologically identical zigzag Ge chains in CaGe.[51] More pronounced π interactions were observed for Ge−Ge dumbbells in different binary and ternary germanides, such as AE_7Ge_6 (AE = Ba, Sr),[52] $La_4Mg_5Ge_6$,[8] $Gd_4Zn_5Ge_6$,[53] and Gd_2MgGe_2.[54]

The COHP curve of Ge−Ge (3b-) interaction states is spread over a larger energy region (starting from about −12.5 eV) and changes its character from bonding to antibonding type only close to E_F.

The character of La−Ge interactions (Figure 10c) becomes of the antibonding type well above E_F, further evidence of the incomplete polarization of La atoms.

The Ge−Ge bonds are associated with the highest −*i*COHP values, which are typical for Ge−Ge covalent interactions.[8,52] These values range from 1.94 to 2.33 eV/bond inside the zigzag chains and from 1.91 to 2.75 eV/bond for the corrugated layers. In each type of Ge-based fragment the −*i*COHP follow the trend of interatomic distances. Within the $[ZnGe_6]^{\delta-}$ covalent network, somewhat weaker interactions are found between Zn and Ge, the corresponding −*i*COHP varying from 1.27 and 1.44 eV/bond. Finally, the numerous La−Ge bonds are associated with lower −*i*COHP values, around 1 eV/bond. Other contacts within the first coodination sphere are irrelevant.

The chemical bonding scenario presented above suggests to describe the $R_2Zn_{1-x}Ge_6$ compounds as near Zintl phases, similar to the closely related $R_2Zn_3Ge_6$ compounds.[2]

4. CONCLUSIONS

The nine new $R_2Zn_{1-x}Ge_6$ compounds (R = La−Nd, Sm, Gd−Ho) were presented in this work, with particular emphasis on their crystal structure peculiarities and regularities in the framework of the ~R_2MGe_6 family (M = transition metal + Mg, Al, Ga). The studied series of intermetallics shows two interesting and peculiar characteristics.

(1) A Zn deficiency regularly increasing with the atomic number of the lanthanide, confirmed both by EDXS measurements and by accurate single-crystal XRD studies. Nevertheless, other Zn-containing intermetallics show a similar deficiency tendency.

(2) A structural change from the orthorhombic structure *o*S72-$Ce_2(Ga_{0.1}Ge_{0.9})_7$ (for R = La−Nd, Sm, Gd, Tb) to the new monoclinic structure *m*P34-$Dy_2Zn_{1-x}Ge_6$ ($x \approx 0.5$, for R = Dy, Ho), which represents an ordered superstructure of the La_2AlGe_6 prototype.

These two structural models are closely related, being characterized by the same Ge-based infinite motifs, namely, 2D zigzag chains and 3D corrugated layers, linked by Zn atoms in slightly different manners. Nonetheless, the heavy R atoms distribution is identical, miming a strong pseudosymmetry

DOI: 10.1021/ic5030313
Inorg. Chem. 2015, 54, 2411−2424

which hampers the correct structural model deduction. This could be the reason why the structure of several R_2MGe_6 compounds, initially reported as *oS*18-Ce_2CuGe_6, was subsequently redetermined as the four times bigger *oS*72-$Ce_2(Ga_{0.1}Ge_{0.9})_7$. From this perspective we think that the structure of many other 2:1:6 phases would need a revision.

Besides the orthorhombic to monoclinic structural change some regularities can be traced along the $R_2Zn_{1-x}Ge_6$ series, depending on the R nature and/or on the Zn content:

(1) the normalized cell volume linearly decreases, reflecting the lanthanide contraction trend, and
(2) the distortion degree of the 3D corrugated layers decreases, due to the always smaller number of capping Zn atoms.

The role of Zn deficiency in governing the structures of the studied compounds motivated us to look for a generalization scheme including vacancy ordering phenomena as a key principle. This goal was achieved within group theory with the help of group−subgroup relations in the *Bärnighausen* formalism. Moreover, this procedure was automated in the ToposPro software package in order to guarantee its completeness.

The resulting scheme is a two-branched *Bärnighausen* tree originating from the $SmNiGe_3$ aristotype via subsequent reduction steps accompanied by vacancy ordering. Within this tree, the 2:1:6 compounds with *oS*72 and *mS*36 structures can be viewed as "isomers" located each on a different branch, both obtained after two reduction steps of the second order but characterized by different vacancy distributions. Growing longer the monoclinic branch from the *mS*36 model, the *mP*34 structure (corresponding to the compound $Dy_2Zn_{1-x}Ge_6 \approx Dy_4ZnGe_{12}$) is obtained via one k2 reduction step along with further vacancy ordering.

The same approach was applied to the $R_2Zn_3Ge_6$ family, enriched during this work with the new Sm and Gd−Ho analogues. A similar two-branched *Bärnighausen* tree was proposed, originating from the $ScNi_2Si_3$ aristotype: two 2:3:6 "isomers" have been particularly derived, having the *oS*44 (reported for the studied $R_2Zn_3Ge_6$ compounds) and *tI*88 (hypothetic) structures. Efforts to obtain the first representative of the latter are in progress.

Finally, structural studies were complemented with electronic calculations performed on the idealized model La_2ZnGe_6, confirming for this series of compounds the existence of a $[ZnGe_6]^{6-}$ polyanionic network counterbalanced by La ions. Therefore, they can be defined as polar intermetallics with near Zintl behavior.

The numerous interesting results presented here trigger several further studies, including the exploration of novel germanides characterized by similar covalent fragments and the revision/expansion of the R_2MGe_6 family of compounds along with quantum chemical analysis in real space according to the quantum theory of atoms in molecules (QTAIM),[55] aiming to a deeper insight into chemical bonding.

■ ASSOCIATED CONTENT

Supporting Information

X-ray crystallographic files in CIF format; SEM/EDXS and XRPD characterization results; interatomic distances; deviation histograms for $Gd_2Zn_{1-x}Ge_6$ single-crystal data; backscattered electron images of alloys surfaces; evolutions of atomic parameters in the *Bärnighausen* formalism between the $SmNiGe_3$ aristotype and $La_2Zn\square Ge_6$ and between the $SmNiGe_3$ aristotype and $Dy_2Zn_{1-x}Ge_6$; evolutions of atomic parameters in the *Bärnighausen* formalism between the $ScNi_2Ge_3$ aristotype and $La_2Zn_3\square Ge_6$; studied structures in terms of linear intergrowth representation; partial DOS curves for La_2ZnGe_6; description of the algorithm of the vacancy ordering modeling in the 2:1:6 family starting from the $SmNiGe_3$ aristotype using ToposPro (the material necessary to reproduce the process is also provided in a separate archive). This material is available free of charge via the Internet at http://pubs.acs.org.

■ AUTHOR INFORMATION

Corresponding Author

*Phone: +39-0103536159. Fax: +39-0103536163. E-mail: pavlo.solokha@unige.it.

Notes

The authors declare no competing financial interest.

■ ACKNOWLEDGMENTS

This research was funded by the University of Genoa within PRA 2013 projects. D.M.P. and V.A.B. thank the Russian government (grant No. 14.B25.31.0005) for support. The authors thank Sergio Fiorito, an undergraduate student, for his contribution to this research in an early stage.

■ REFERENCES

(1) Zhang, J.; Tobash, P. H.; Pryz, W. D.; Buttey, D. J.; Hur, N.; Thompson, J. D.; Sarrao, J. L.; Bobev, S. *Inorg. Chem.* **2013**, *52*, 953−964.
(2) Salvador, J. R.; Gour, J. R.; Bilc, D.; Mahanti, S. D.; Kanatzidis, M. G. *Inorg. Chem.* **2004**, *43*, 1403−1410.
(3) Peter, S. C.; Sarkar, S.; Kanatzidis, M. G. *Inorg. Chem.* **2012**, *51*, 10793−10799.
(4) De Negri, S.; Solokha, P.; Skrobańska, M.; Proserpio, D. M.; Saccone, A. *J. Solid State Chem.* **2014**, *218*, 184−195.
(5) Zhang, J.; Wang, Y.; Bobev, S. *Inorg. Chem.* **2015**, *54*, 722−732.
(6) Peter, S. C.; Chondroudi, M.; Malliakas, C. D.; Balasubramanian, M.; Kanatzidis, M. G. *J. Am. Chem. Soc.* **2011**, *133*, 13840−13843.
(7) Kraft, R.; Pöttgen, R. *Monatsh. Chem.* **2004**, *135*, 1327−1334.
(8) Solokha, P.; De Negri, S.; Skrobanska, M.; Saccone, A.; Pavlyuk, V.; Proserpio, D. M. *Inorg. Chem.* **2012**, *51*, 207−214.
(9) Fukuoka, H.; Yoshikawa, M.; Baba, K.; Yamanaka, S. *Bull. Chem. Soc. Jpn.* **2010**, *83*, 323−327.
(10) Zhuravleva, M. A.; Robert, D. B.; Pcionek, J.; Mahanti, S. D.; Kanatzidis, M. G. *Inorg. Chem.* **2005**, *44*, 2177−2188.
(11) Salvador, J. R.; Bilc, D.; Gour, J. R.; Mahanti, S. D.; Kanatzidis, M. G. *Inorg. Chem.* **2005**, *44*, 8670−8679.
(12) Pecharsky, V. K.; Gschneidner, K. A. *Phys. Rev. Lett.* **1997**, *78*, 4494−4497.
(13) Majumdar, S.; Sampathkumaran, E. V. *Phys. Rev. B* **2001**, *63* (172407), 1−4.
(14) Johrendt, D.; Hosono, H.; Hoffman, R. D.; Pöttgen, R. *Z. Kristallogr.* **2011**, *226*, 435−446.
(15) Müller, U. *Symmetry Relationships between Crystal Structures. Applications of Crystallographic Group Theory in Crystal Chemistry*; Oxford University Press: New York, 2013.
(16) Villars, P.; Cenzual, K. Pearson's Crystal Data, Release 2013/14, ASM International, Ohio, USA.
(17) Salamakha, P. S.; Sologub, O. L.; Bodak, O. I. In *Handbook on the Physics and Chemistry of Rare Earths*; Gschneidner, K. A., Jr., Eyring, L., Eds.; Elsevier Science B.V.: Amsterdam, 1999; Vol. 27, Chapter 173 (Ternary rare-earth-germanium systems), pp 204−214.
(18) Gribanov, A.; Safronov, S.; Murashova, E.; Seropegin, Y. *J. Alloys Compd.* **2012**, *542*, 28−31.

DOI: 10.1021/ic5030313
Inorg. Chem. 2015, 54, 2411−2424

(19) Fornasini, M. L.; Manfrinetti, P.; Palenzona, A. *Z. Kristallogr. NCS* **2002**, *217*, 173−174.
(20) Tokaychuk, Y. O.; Filinchuk, Y. E.; Fedorchuk, A. O.; Kozlov, A. Yu.; Mokra, I. R. *J. Solid State Chem.* **2006**, *179*, 1323−1329.
(21) Zhao, J. T.; Cenzual, K.; Parthè, E. *Acta Crystallogr., Sect. C* **1991**, *47*, 1777−1781.
(22) Grin, Yu. The intergrowth concept as a useful tool to interpret and understand complicated intermetallic structures. In *Modern Perspectives in Inorganic Crystal Chemistry*, Parthè, E., Ed.; Kluwer Academic Publishers: Norwell, MA, 1992; pp 77−95.
(23) Bruker. *APEX2, SAINT-Plus, XPREP and SADABS*; Bruker AXS Inc.: Madison, WI, 2014.
(24) Blatov, V. A.; Shevchenko, A. P.; Proserpio, D. M. *Cryst. Growth Des.* **2014**, *14*, 3576−3586.
(25) Krier, G.; Jepsen, O.; Burkhardt, A.; Andersen, O. K. *TB-LMTO-ASA program*, version 4.7; Max-Planck-Institut für Festkörperforschung: Stuttgart, Germany, 1994.
(26) Dronskowski, R.; Blöchl, P. E. *J. Phys. Chem.* **1993**, *97*, 8617−8624.
(27) Blöchl, P. E.; Jepsen, O.; Andersen, O. K. *Phys. Rev. B* **1994**, *49*, 16223−16233.
(28) Eck, B. *wxDragon*; Aachen, Germany, 1994−2014; http://wxdragon.de.
(29) Petricek, V.; Dusek, M.; Palatinus, L. *Z. Kristallogr.* **2014**, *229*, 345−352.
(30) Sheldrick, G. M. *Acta Crystallogr., Sect. A* **2008**, *64*, 112−122.
(31) Farrugia, L. J. *J. Appl. Crystallogr.* **2012**, *45*, 849−854.
(32) Reker, B.; Johrendt, D.; Pöttgen, R. *Intermetallics* **2013**, *38*, 36−43.
(33) Gelato, L. M.; Parthé, E. *J. Appl. Crystallogr.* **1987**, *20*, 139−143s.
(34) Zhao, J. T.; Cenzual, K.; Parthè, E. *Acta Crystallogr., Sect. C* **1991**, *47*, 1777−1781.
(35) Peter, S. C.; Chondroudi, M.; Malliakas, C. D.; Balasubramanian, M.; Kanatdidis, M. G. *J. Am. Chem. Soc.* **2011**, *133*, 13840−13843.
(36) Christensen, J.; Lidin, S.; Malaman, B.; Venturini, G. *Acta Crystallogr., Sect. B* **2008**, *64*, 272−280.
(37) Zhang, J.; Tobash, P. H.; Pryz, W. D.; Buttey, D. J.; Hur, N.; Thompson, J. D.; Sarrao, J. L.; Bobev, S. *Inorg. Chem.* **2013**, *52*, 953−964.
(38) Carrillo-Cabrera, W.; Budnyk, S.; Prots, Y.; Grin, Y. *Z. Anorg. Allg. Chem.* **2004**, *630*, 2267−2276.
(39) Kirsanova, M. A.; Mori, T.; Maruyama, S.; Matveeva, M.; Batuk, D.; Abakumov, A. M.; Gerasimenko, A. V.; Olenev, A. V.; Grin, Y.; Shevelkov, A. V. *Inorg. Chem.* **2013**, *52*, 577−588.
(40) Thimmaiah, S.; Miller, G. J. *Inorg. Chem.* **2013**, *52*, 1328−1337.
(41) Mizutani, U. *Hume-Rothery rules for structurally complex alloy phases*; CRC Press, Taylor & Francis Group: Boca Raton, FL, 2010.
(42) Parthé, E.; Chabot, B. A.; Cenzual, K. *Chimia* **1985**, *39*, 164−174.
(43) Parthé, E.; Gelato, L.; Chabot, B.; Penzo, M.; Cenzual, K.; Gladyshevskii, R. *TYPIX Standardized Data and Crystal Chemical Characterization of Inorganic Structure Types*, 8th ed.; Springer Verlag: New York, 1993.
(44) Aroyo, M. I.; Perez-Mato, J. M.; Orobengoa, D.; Tasci, E.; de la Flor, G.; Kirov, A. *Bulg. Chem. Commun.* **2011**, *43*, 183−197.
(45) Klemm, W.; Busmann, E. *Z. Anorg. Allg. Chem.* **1963**, *319*, 297−305.
(46) Müller, U. *Inorganic Structural Chemistry*, 2nd ed.; John Wiley& Sons Ltd.: New York, 2006.
(47) Stegmaier, S.; Fässler, T. *J. Solid State Chem.* **2012**, *192*, 312−324.
(48) Haussermann, U.; Amerioun, S.; Eriksson, L.; Lee, C. S.; Miller, G. J. *J. Am. Chem. Soc.* **2002**, *124*, 4371−4383.
(49) Li, B.; Corbett, J. D. *Inorg. Chem.* **2006**, *45*, 8958−8964.
(50) Lin, Q.; Corbett, J. D. *J. Am. Chem. Soc.* **2007**, *129*, 6789−6797.
(51) Miller, G. J. Structure and Bonding at the Zintl Border. In *Chemistry, Structure, and Bonding of Zintl Phases and Ions*; Kauzlarich, S. M., Ed.; VCH Publishers, Inc.: New York, 1996; pp 1−55.
(52) Siggelkow, L.; Hlukhyy, V.; Fässler, T. F. *J. Solid State Chem.* **2012**, *191*, 76−89.
(53) Kranenberg, C.; Johrendt, D.; Mewis, A. *Z. Anorg. Allg. Chem.* **2001**, *627*, 539−544.
(54) Choe, W.; Miller, G. J.; Levin, E. M. *J. Alloys Compd.* **2001**, *329*, 121−130.
(55) Bader, R. F. W. *Atoms in Molecules: A Quantum theory*; Clarendon Press: Oxford, U.K., 1990.

NOTE ADDED AFTER ASAP PUBLICATION

This paper was published ASAP on February 10, 2015. Tables 1 and 2 were updated. The revised paper was reposted on February 18, 2015.

DOI: 10.1021/ic5030313
Inorg. Chem. 2015, 54, 2411−2424